PHYSICAL REVIEW B VOLUME 35, NUMBER 12 15 APRIL 1987-II

Electronic transport in a superlattice with average periodic order

Nandini Trivedi and N. W. Ashcroft
Laboratory of Atomic and Solid State Physics, Cornell University, Ithaca, New York 14853-2501
(Received 21 July 1986; revised manuscript received 15 December 1986)

We introduce a model to describe scattering from disordered metallic interfacial regions in layered structures, or superlattices. This model is also applicable to interface roughness or boundary scattering in single junctions. It consists of an array of slabs of scattering centers embedded in a host metal. The slabs have thickness t and are separated by a distance d. Each simulates an interfacial region in which the physical arrangement of scattering centers is disordered with positional correlations *within* a slab being represented by a structure factor S, but atomic positions being uncorrelated *between* slabs. For a description of the structure factor of a slab with assumed *quenched* disorder, the pair correlation function for homogeneous liquids is used as an input after extension both to finite geometry and into regions of high density typical of solids. The Boltzmann equation, with the anisotropic structural information incorporated in the collision term, is solved by a variational principle, and yields the in-plane and out-of-plane resistivity and thermopower components as functions of d, t, and the density of scattering centers in a slab. The results show that it is possible to characterize the microscopic structural features of the interfacial region in terms of the transport properties of the system.

I. INTRODUCTION

Studies on surfaces and interfaces are growing in importance primarily because of the corresponding development of tools and techniques to fabricate and probe these structures. It is now possible to obtain detailed information on a wide range of interface properties including the microscopic structure, chemical composition, atomic bonding, presence of defects and misfit dislocations, interface chemical reactions, and interdiffusion. The metal-semiconductor interface[1] and its role in Schottky-barrier formation, for example, has been actively studied because of its importance in device applications. More recently, with further advances in thin-film deposition techniques it has become possible to synthesize modulated structures with a high degree of structural and chemical order.[2] Layered structures of total film thickness of ~ 1 μm containing individual layers of thickness in the range 5—5000 Å have been prepared. These structures, which include metallic[3–6] and semiconductor superlattices,[7] usually consist of alternating layers of two primary constituents. The modulation period of superlattices can even be tailored to be smaller than the effective electron mean free path. Under such conditions, the transport characteristics are dominated by scattering at the array of interfaces formed at the junctions of the two constituents. An important question therefore, for both single metal-semiconductor junctions and modulated structures, is the relationship of the microscopic interfacial structure to the macroscopic transport properties.

A major source of interfacial disorder is interdiffusion between the two constituents on either side of the junction; it is this issue that we address here rather than the role of Schottky or other related barriers. For example, in metal-semiconductor junctions, intermixed regions of order 10^2 Å, formed by diffusion along grain boundary paths, have been reported.[8] X-ray diffraction studies of metallic superlattices, which show long-range structural coherence perpendicular to the layers[3] for layer thicknesses greater than ~ 10 Å, also establish that interdiffusion[5] can occur over a distance of the order of ~ 15 Å. Transport measurements of the in-plane resistivity versus modulation period in metallic superlattices have also recently been reported.[9,10] These experiments have largely been interpreted according to the finite-size-effect theory of Fuchs[11] and Sondheimer[12] in which the effect of diffuse scattering at a boundary is included via a phenomenological specularity parameter p. The calculation we shall present below is a first step toward an understanding of the *correlation* between the *microscopic* structural features of the interfacial region or of the boundary with the transport properties of the system. We repeat that we shall be dealing exclusively with metallic environments.

Toward this end, we introduce a model to study scattering from disordered interfacial regions of *finite* thickness in such a heterostructure and obtain the in-plane and out-of-plane components of the resistivity and thermopower, which are in principle a direct probe of the interfacial disorder, as we shall see. The model consists of periodically repeated replicas of slabs embedded in a host metal. The physical arrangement of atoms within a slab is disordered but highly correlated at short range. The distance between slabs, d, is taken to be less than the mean free path of electrons in the host metal; transport characteristics of the system are therefore determined primarily by the properties of the disorder of a given slab. In our analysis we include positional correlations between the atoms within a slab (intraslab) but neglect any correlation between atoms in *different* slabs (interslab), an approximation that is reasonable since, as noted, d is typically much greater than the thickness of an individual slab. Upon

averaging over the disorder, this ansatz leads to average periodic order in one dimension along the superlattice axis. Physical disorder *within* a slab is approximated by a *quenched* distribution of scattering centers, described by single-particle and two-particle densities, that are functions of the position of ions in a slab. The justification for this approximation is that the heterostructures mentioned above are often grown by molecular-beam epitaxy or sputtering techniques which involve the emission of atoms (constituents of the heterostructure) from a source and their subsequent rapid condensation on a substrate. The substrate acts as an effective heat bath dissipating the excess energy in the atoms and in turn produces a structure in the interface region with various degrees of order. For the disordered cases we describe the structure by the equivalent of a frozen liquid.

In the literature,[13,14] calculations of the resistivity of metals in the presence of impurities have usually assumed a uniform distribution of scatterers. While this is a good approximation for low impurity density, it fails at higher densities when the average spacing between the impurities becomes of the order of the range of the interimpurity potential. In interdiffused regions, the concentration of the diffusing species spans the entire range from low to high concentrations. In view of this, we retain information at least up to the two-particle density, which is a measure of pair correlations between the atoms. In the *theory of homogeneous liquids*[15] the analogous problem of determining the pair correlation function, given an interatomic potential, has been studied in great detail, and in the approximation used here, is extended into regions of higher density, characteristic of solids, to describe the structure of a disordered interface. We use this liquid-state correlation function as input to obtain approximate expressions for the two-particle correlation function for scattering centers in a finite slab geometry.

The structural information described above is used in the collision term of the linearized Boltzmann equation in a weak electric field. The spatial arrangement of atoms within a slab and the periodic arrangement of slabs in one dimension contribute to the *total* scattering potential in this model. In spite of the fact that the potential of a single ion is isotropic, the total scattering potential in which the structural features of an interface are included, is anisotropic. Such an anisotropic collision kernel does not lead to a solution of the Boltzmann equation based on the usual relaxation-time-approximation approach. We show in Sec. II, that in the presence of anisotropy, the modes of the distribution function are coupled and a relaxation time independent of the distribution function cannot therefore be obtained. For this reason we resort to a variational solution of the Boltzmann equation which provides a well-known bound on the transport coefficients. In Sec. III we formulate the replicated slab model in detail to describe scattering from disordered interfaces and discuss approximations to the pair correlation function in a finite geometry. Our results for the resistivity and thermopower components are presented in Sec. IV. The specific heterostructure studied here consists of aluminum which provides the host environment and tetravalent ions (e.g., Si) embedded in a metallic Al matrix which form the disordered interface. As will be seen, the behavior of the in-plane resistivity as a function of the modulation period of the superlattice agrees with measurements on metallic superlattices. In addition, we give predictions for the behavior of both the in-plane and the out-of-plane components of the resistivity and the thermopower tensor as functions of the degree of disorder and thickness of the interfacial region, measurements of which have so far not been reported. The relevance of these results to experiments along with other applications are discussed in Sec. V.

II. TRANSPORT COEFFICIENTS VIA THE BOLTZMANN EQUATION

A. Limitations of the relaxation-time approximation

The non-equilibrium electronic distribution function $g(\mathbf{r},\mathbf{k},t)$ satisfies the Boltzmann equation

$$\frac{\partial g}{\partial t}+\mathbf{v}\cdot\nabla_r g+\mathbf{F}\cdot\nabla_k g=\left[\frac{\partial g}{\partial t}\right]_{\text{coll}}, \tag{2.1}$$

where $\mathbf{F}$ contains the applied external forces and the right-hand side of (2.1) is the rate of change of the non-equilibrium distribution function attributable to collisions. For elastic scattering, this collision term is given by[16]

$$\left[\frac{\partial g(\mathbf{k})}{\partial t}\right]_{\text{coll}}=-\sum_{\mathbf{k}'} W_{\mathbf{k}\mathbf{k}'}[g(\mathbf{k})-g(\mathbf{k}')], \tag{2.2}$$

where $W_{\mathbf{k}\mathbf{k}'}$ is the transition rate from state $\mathbf{k}$ to $\mathbf{k}'$. In Sec. III, we evaluate the transition rate for a replicated slab model that describes scattering from disordered interfaces. In this model, anisotropy arises from the physical arrangement of scattering centers in the interface. With this in mind, secondary sources of anisotropy, such as band structure, are neglected in the following discussion. Our conclusions regarding the limitations of the relaxation-time approximation, however, remain unchanged even with the inclusion of nonspherical Fermi surfaces.

For the familiar case of *isotropic* scattering, $W_{\mathbf{k}\mathbf{k}'}$ depends *only* on the angle between the vectors $\mathbf{k}$ and $\mathbf{k}'$, and we can expand both the transition rate and the distribution function in spherical harmonic basis functions with expansion coefficients ω_l and f_{lm}, respectively. Thus,

$$W_{\mathbf{k}\mathbf{k}'}=\delta(\varepsilon_{\mathbf{k}}-\varepsilon_{\mathbf{k}'})\sum_l \omega_l(\varepsilon_{\mathbf{k}})P_l(\hat{\mathbf{k}}\cdot\hat{\mathbf{k}}') \tag{2.3}$$

and

$$g(\mathbf{k})=\sum_{l,m} f_{lm}(\varepsilon_{\mathbf{k}})Y_{lm}(\Omega), \tag{2.4}$$

where $P_l(\cos\theta)$ are the Legendre polynomials and $Y_{lm}(\Omega)$, the spherical harmonics. Using standard properties of spherical harmonics, (2.2) reduces to[17]

$$\left[\frac{\partial f_{lm}}{\partial t}\right]_{\text{coll}}=-\frac{f_{lm}}{\tau_l}, \tag{2.5}$$

where τ_l is given by

$$\frac{1}{\tau_l}=N(\varepsilon_{\mathbf{k}})\Omega\left[\omega_0-\frac{\omega_l}{2l+1}\right]. \tag{2.6}$$

In (2.6), Ω is the volume of the system, $N(\varepsilon_{\mathbf{k}})=N(\varepsilon_F)(\varepsilon_{\mathbf{k}}/\varepsilon_F)^{1/2}$ and $N(\varepsilon_F)$ is the free-electron density of levels per spin at the Fermi energy. Note that $1/\tau_0$ vanishes, which is equivalent to the statement that the number of particles is conserved in collisions.

From (2.5) we immediately conclude that when the perturbing field is removed, each mode (labeled by $\{l,m\}$), relaxes independently to equilibrium. Furthermore, the characteristic relaxation time of a mode is *independent* of the distribution function, as seen from (2.6). Accordingly, from (2.1) we find that *each mode* satisfies a separate Boltzmann equation with a collision term such that the relaxation-time approximation is exact (for that mode). In special cases when either (i) there is a single mode in the system, or (ii) all the modes relax with the same time constant,[18] the collision term for the total distribution function $g(\mathbf{k})$ can be described exactly by the relaxation-time approximation.

For an *anisotropic* collision kernel (as will be shown in Sec. III to arise in the problem of scattering from a disordered interface), the transition rate requires an expansion in a double spherical harmonic series. From an analysis similar to the one above, we find that the relaxation rate of a given mode is coupled to *all* other modes in the system [see (A4) and (A6)], and as a consequence, a solution of the Boltzmann equation cannot be readily obtained within the relaxation-time approximation. Alternatively, if we insist that in an anisotropic system the total distribution function relax exponentially to equilibrium with a time constant $\tau(\mathbf{k})$ that has angular dependence, we find that a solution of (2.2) leads to a constraint on the sum of the expansion coefficients of τ. It is, however, not possible to determine the individual coefficients [see (A10)]. In general, it is not possible to obtain a scattering time $\tau(\mathbf{k})$ in terms of the transition probability $W_{\mathbf{k}\mathbf{k}'}$ given by a microscopic theory, in such a way that the scattering time is *also* independent of the distribution function g [see (A6)].

Anisotropic transition probabilities arising from band-structure effects in metals (e.g., Al, Cu, and substitutional alloys) have been studied by several authors.[19–22] In these systems the electron-ion pseudopotential is spherically symmetric and it is possible to describe the scattering in terms of a finite number of phase shifts. The collision kernel in the Boltzmann equation is then reducible to the degenerate form for which an exact solution can be obtained as shown by Sondheimer.[23] However, in the model that we discuss in Sec. III, the total scattering potential is anisotropic and an expansion in terms of phase shifts is not valid.

B. Variational principle

As shown above, the standard procedures to solve the Boltzmann equation, in a system with an anisotropic total scattering potential, are not immediately applicable and a variational approach to the problem is therefore indicated. It can be shown that there exists a variational function $\rho_{\hat{\mathbf{n}}\hat{\mathbf{n}}}^{\text{trial}}$ for the linearized Boltzmann equation, which is a functional of an arbitrary trial function $\Phi_{\hat{\mathbf{n}}}(\mathbf{k})$, and is in fact an upper bound on the true value of the electrical resistivity,[24]

$$\rho_{\hat{\mathbf{n}}\hat{\mathbf{n}}}\le\rho_{\hat{\mathbf{n}}\hat{\mathbf{n}}}^{\text{trial}}=\frac{\sum_{\mathbf{k}\mathbf{k}'}\Phi_{\hat{\mathbf{n}}}(\mathbf{k})W_{\mathbf{k}\mathbf{k}'}\Phi_{\hat{\mathbf{n}}}(\mathbf{k}')(-\partial g^0/\partial\epsilon_{\mathbf{k}})}{\left[\sum_{\mathbf{k}}\mathbf{v}_{\hat{\mathbf{n}}}(\mathbf{k})\Phi_{\hat{\mathbf{n}}}(\mathbf{k})(-\partial g^0/\partial\varepsilon_{\mathbf{k}})\right]^2}, \tag{2.7}$$

where $\hat{\mathbf{n}}$ is a unit vector in the direction of a constant electric field $\mathbf{E}$. To determine the least upper bound on ρ, Φ is expanded in a set of N spherical harmonics, and the variational function is minimized with respect to the expansion coefficients. The expression so obtained [see (B2)], requires the inversion of an $N\times N$ matrix which in turn contains the elements of the transition probability $W(lm;l'm')$ defined in (B5). Given the geometry of the model, it is easy to show from (B2) that for an isotropic dispersion relation obeyed by the electrons, the two independent components of the resistivity tensor are related to only two basic matrix elements of W. The components ρ_{zz} and ρ_{xx} are found to be inversely proportional to $W^{-1}(1,0;1,0)$ and $W^{-1}(1,1;1,-1)$, respectively, with the same prefactor [see (4.5)]. In the isotropic limit, the two resistivity components become equal and the resistivity reduces to the expression familiar in the theory of liquid metals.[25] [Appendix B and (4.6).]

To obtain the thermopower, we consider a situation in which a temperature gradient is applied in the presence of an electric field. Within the assumption of linear response, the current obtained is

$$\mathbf{J}=\overleftrightarrow{L}_{EE}\cdot\mathbf{E}+\overleftrightarrow{L}_{ET}\cdot(-\nabla T), \tag{2.8}$$

where, in general, $\overleftrightarrow{L}_{EE}$ and $\overleftrightarrow{L}_{ET}$ are tensors. The thermopower is defined as the electrostatic potential developed across the system in a unit thermal gradient, when no electric current is allowed to flow, and is given by

$$\overleftrightarrow{Q}=(\overleftrightarrow{L}_{EE})^{-1}\cdot\overleftrightarrow{L}_{ET}. \tag{2.9}$$

For a system with tetragonal symmetry, as considered in this paper (see Fig. 1), the tensors in (2.8) are diagonal with their xx and yy components equal but different from the zz component and this symmetry is also reflected in the thermopower tensor. A generalization of the variational approach used to evaluate the resistivity above, is developed to obtain the thermopower. However, the expression for the thermopower is rather complicated, as can be seen even in the simple case considered by Ziman[26] with only two terms retained in the expansion of the distribution function. However, in the event that the scattering by quenched scattering centers is elastic [see (2.2)], the Wiedemann-Franz law holds[27] and the variational solution of the thermopower simplifies to

$$Q_{\mu\mu}=-\frac{\pi^2k_B^2T}{3\,|\,e\,|\,\varepsilon_F}\left[\varepsilon\frac{\partial\ln\sigma_{\mu\mu}(\varepsilon)}{\partial\varepsilon}\right]_{\epsilon=\varepsilon_F}. \tag{2.10}$$

It is important that the term in large parentheses, denoted by $\xi_{\mu\mu}$, be correctly interpreted. It is the variation of a function $\sigma(\varepsilon)$, evaluated on an arbitrary energy shell ε, with respect to ε *at a constant electron density*. The func-

tion $\sigma(\varepsilon)$ is the physically measurable conductivity only at ε_F. When applied to the replicated slab model, the thermopower is found to be related to the matrix elements of the transition probability W and to their derivative with respect to ε. Again on symmetry grounds, ξ_{zz} and ξ_{xx} are related to the (1,0;1,0) and (1,1;1,−1) elements of W, respectively. Finally, the isotropic limit is easily recovered (Appendix C) and agrees with the standard expression for the thermopower in liquid metals.[28]

III. FORMALISM

A. Replicated slab model

The replicated slab model introduced qualitatively in Sec. I, as a description of disordered interfacial regions in a modulated structure, is now developed quantitatively. The model consists of an array of M slabs each containing N ions, embedded in a host metal, the host determining the average electron density. These slabs are arranged periodically with period d in one dimension as depicted in Fig. 1.

The Hamiltonian for our system is given within the independent-particle approximation by

$$H = H_{\text{host}} + V \ , \tag{3.1}$$

where H_{host} describes the electrons in the host metal and satisfies the eigenvalue equation

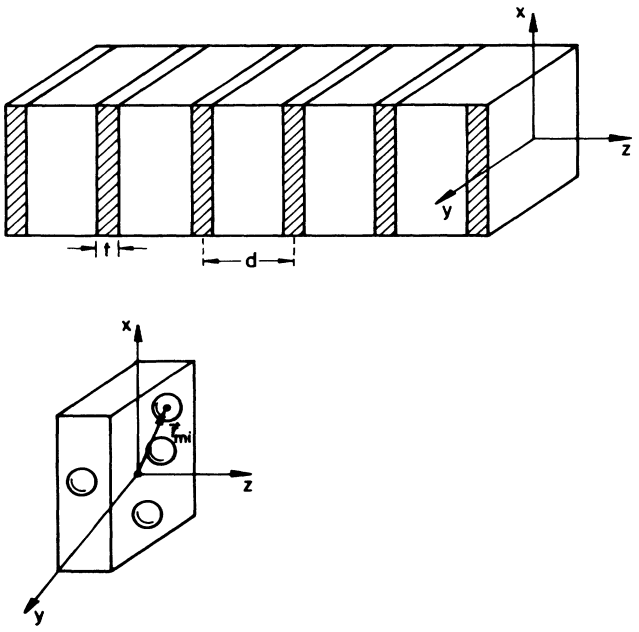

FIG. 1. The replicated slab model consists of an array of M slabs (shown hatched), each of thickness t and area A embedded in a host metal. The modulation period of this structure is d. The slabs contain a distribution of N atoms and r_{mi} denotes the position of the ith atom in the mth slab. The superlattice axis is chosen along the z direction. The specific system considered is a metallic heterostructure with Al as the host metal and tetravalent scattering centers, e.g., Si embedded in a metallic environment forming the disordered slabs.

$$H_{\text{host}} \mid \mathbf{k} \rangle = \varepsilon_{\mathbf{k}} \mid \mathbf{k} \rangle \ . \tag{3.2}$$

We have assumed for simplicity that the host metal can be described as a free-electron single-band metal with a spherical Fermi surface. The total electron-ion potential V in (3.1) furnished by the ions in the array of slabs can be explicitly written as

$$V = \sum_{m=1}^{M} \sum_{i=1}^{N} U[\mathbf{r} - (md\hat{\mathbf{z}} + \mathbf{r}_{mi})] \ , \tag{3.3}$$

where $\mathbf{r}_{mi}$ is the position of the ith ion in the mth slab and $U(\mathbf{r})$ is a spherically symmetric pseudopotential describing the potential of a single ion with interactions between electrons, included in it self-consistently.

We first show that the average over the disorder of the total electron-ion potential is periodic along the superlattice axis, chosen to be the z direction. The potential in (3.3) is written in terms of its Fourier components and an average over the positions of the ions in the slabs, denoted by angular brackets, is performed. We obtain

$$\langle V(\mathbf{r}) \rangle = \sum_{m=1}^{M} \int \frac{d^3k}{(2\pi)^3} e^{i\mathbf{k}\cdot(\mathbf{r} - md\hat{\mathbf{z}})} U(\mathbf{k}) n(-\mathbf{k}) \ , \tag{3.4}$$

where the Fourier transform of the single particle density operator is defined as

$$\hat{n}_m(\mathbf{k}) = \sum_{i \in m\text{th slab}} e^{i\mathbf{k}\cdot\mathbf{r}_{mi}} \ . \tag{3.5}$$

In obtaining (3.4) we have also assumed that the slabs are statistically identical, so that the average of (3.5), denoted by $n(\mathbf{k})$, is independent of the slab index m. From (3.4) it is straightforward to obtain

$$\langle V(r) \rangle = \sum_{m=1}^{M} P(\mathbf{r}_\perp, z - md) \ , \tag{3.6}$$

which is periodic in the z direction with period d. In (3.6), $P(\mathbf{r})$ is the Fourier transform of $P(\mathbf{k}) = U(\mathbf{k}) n(-\mathbf{k})$ and $\mathbf{r}_\perp$ is a vector in the x-y plane. The Hamiltonian in (3.1) can be rewritten as

$$H = H_0 + \Delta V \ , \tag{3.7}$$

where $H_0 = H_{\text{host}} + \langle V \rangle$ is the sum of the Hamiltonian of the host metal and the average of the superlattice potential and $\Delta V = V - \langle V \rangle$, is the deviation of the superlattice potential from its average value. Furthermore, we shall assume that ΔV is a weak perturbation[29] on H_0; this is the essential approximation which allows the fundamental transition rate to be evaluated within Born approximation. For elastic scattering of an electron from level $\mathbf{k}$ to level $\mathbf{k}'$, this rate is given by

$$W_{\mathbf{k}\mathbf{k}'} = \frac{2\pi}{\hbar} \mid \Delta V_{\mathbf{k}\mathbf{k}'} \mid^2 \delta(\varepsilon_{\mathbf{k}} - \varepsilon_{\mathbf{k}'}) \ . \tag{3.8}$$

The eigenstates of H_0 in (3.7) are comprised of plane waves in the x-y plane (for a free-electron metal) and Bloch waves in the z direction. This is a consequence of the one-dimensional periodic potential provided by the superlattice *on average*. However, for typical modulation periods $d \sim 20$–100 Å, any deviation in the dispersion of the host metal arising from the periodic superlattice po-

tential can be neglected.[30] The matrix elements in (3.8) are then functions only of $\mathbf{k}-\mathbf{k}'=\mathbf{q}$ and we have

$$V_{\mathbf{k}\mathbf{k}'}=\frac{1}{\Omega}V(\mathbf{q})=\frac{1}{\Omega}\int d^3r\, e^{i(\mathbf{k}-\mathbf{k}')\cdot\mathbf{r}}V(\mathbf{r}) , \tag{3.9}$$

where Ω is the volume of the system and $V(\mathbf{q})$ is the Fourier transform of the superlattice potential in (3.3) given by

$$V(\mathbf{q})=U(\mathbf{q})\sum_m \hat{n}_m(-\mathbf{q})e^{-iq_z md} , \tag{3.10}$$

where $\hat{n}_m(\mathbf{q})$ is defined in (3.5) and $U(\mathbf{q})$ is the Fourier transform of the single-ion potential.

To obtain the disorder-averaged transition rate $\langle W_{\mathbf{k}\mathbf{k}'}\rangle$, we need to determine $\langle |V(\mathbf{q})|^2\rangle$. From (3.10) we find

$$\langle |V(\mathbf{q})|^2\rangle = |U(\mathbf{q})|^2 \sum_{m=1}^{M}\sum_{m'=1}^{M} e^{-iq_z(m-m')d} \times\langle \hat{n}_m(-\mathbf{q})\hat{n}_{m'}(\mathbf{q})\rangle . \tag{3.11}$$

The average of the two-particle operator in (3.11) is evaluated by making two plausible assumptions: (i) that the slabs are statistically independent (i.e., there are no correlations between the positions of scattering centers in different slabs); the average in (3.11) then reduces to an average of the two-particle operator within a single slab if the slab indices m and m' are identical; and if not, to the product of the average of single-particle operators, and (ii) that the slabs are statistically identical [which implies that the average over the disorder performed in step (i) is independent of the slab index]. The average in (3.11) then reduces to

$$\langle |V(\mathbf{q})|^2\rangle = |U(\mathbf{q})|^2\left[MNS(\mathbf{q})+M^2\langle\hat{n}(\mathbf{q})\rangle\langle\hat{n}(-\mathbf{q})\rangle\sum_G \delta_{q_z,G}\right] , \tag{3.12}$$

where G is a reciprocal superlattice vector (and equals $2\pi l/d$, where l is an integer between 1 and M) in the z direction, arising from the average periodicity of the positions of the slabs. In (3.12), $S(\mathbf{q})$ is the static structure factor of a single slab as defined by

$$S(\mathbf{q})=\frac{1}{N}[\langle\hat{n}(\mathbf{q})\hat{n}(-\mathbf{q})\rangle-\langle\hat{n}(\mathbf{q})\rangle\langle\hat{n}(-\mathbf{q})\rangle] , \tag{3.13}$$

with the angular brackets now implying an average over all positions of the N atoms within a *single* slab. The second term in (3.12) can be identified as $|\langle V(\mathbf{q})\rangle|^2$. On substituting (3.12) in (3.8) and using

$$\langle|\Delta V_{\mathbf{k}\mathbf{k}'}|^2\rangle=\frac{1}{\Omega^2}[\langle|V(\mathbf{q})|^2\rangle-|\langle V(\mathbf{q})\rangle|^2] , \tag{3.14}$$

the average transition rate reduces to

$$\langle W_{\mathbf{k}\mathbf{k}'}\rangle=\frac{2\pi}{\hbar}\frac{MN}{\Omega^2}|U(\mathbf{q})|^2S(\mathbf{q})\delta(\varepsilon_{\mathbf{k}}-\varepsilon_{\mathbf{k}'}) . \tag{3.15}$$

Since we have neglected any correlation between atoms in different slabs, the total scattering is M times the scattering from a single slab. Such a decoupling suggests that it is also possible to treat within this model the scattering from a *single* interface or grain boundary. The problem of a single junction simply consists of a host metal containing within it a slab of atoms whose positions are disordered (the interface). To treat the scattering from the slab atoms, we need to perturb around the eigenstates of the electrons in the host metal which are best described by box eigenfunctions. Such an ansatz for the eigenstates is, however, not useful if the interest is in studying transport properties. To avoid this problem we use a repeated array of replicas of a single slab, for which we are now justified in using plane waves as the unperturbed eigenstates. It is clear that the problem of scattering from a single slab is then replaced by the problem of scattering from an array of slabs which are identical *only on average*, with the spacing between slabs so chosen, that the scattering from different slabs is uncorrelated. Finally, in general, the structure factor in a finite geometry is a function of two arguments $S(\mathbf{q},\mathbf{q}')$, as will be seen in Sec. III B; however, since in the evaluation of the transition rate, matrix elements are computed between plane-wave states, we need to retain only the diagonal term in S. In the following section, we discuss in detail the structure factor in a finite slab geometry.

B. Structure factor in a finite geometry

For any operator $\hat{O}$ [e.g., the two-particle operator in (3.13)], the angular brackets are explicitly defined by an average over all positions of the N atoms within a slab weighted by a quenched probability density. Within Born approximation, as seen from (3.13), only information up to the two-particle density operator needs to be retained. As discussed in the Introduction, a description of pair correlations between scattering centers that are quenched in a slab is developed by using the known pair distribution function $S(q,\eta)$ of atoms in a homogeneous liquid, interacting via hard-sphere potentials.[31] For a homogeneous liquid, S depends only on the magnitude of $\mathbf{q}$ and the packing fraction η is the fraction of the total volume occupied by the atoms and equals $\eta=\frac{4}{3}\pi(\sigma/2)^3n_0$, where n_0 is the number density and σ the diameter of the atoms. In an effort to extend the structure factor of a liquid (known in the thermodynamic limit) to a finite geometry, we obtain approximations to the correlation function in two limiting cases. For a thick slab in which the effective mean free path is less than its thickness t, we calculate corrections of order $1/t^2$ to the bulk value. In the opposite limit we make use of an empirical observation, namely, that the two-dimensional structure factor for hard-disk

interatomic potentials can be obtained to a good approximation by appropriately scaling the *hard-sphere* structure factor. This scaled structure factor is used to describe an atomically abrupt interface. For interfaces a few atomic layers thick, S is found by augmenting the two-dimensional structure factor with Gaussian fluctuations normal to the slab having their origin in physical positional disorder. Note that the correlation function in a homogeneous liquid can be analytically extended to densities considerably higher than those of fluids and are thus applicable to a description of the disorder present in an interface at densities characteristic of solids.
terface at densities characteristic of solids.

To obtain the structure factor for a slab, we start with the two-particle density operator defined by

$$\hat{n}_2(\mathbf{r},\mathbf{r}')=\sum_i \sum_{j\neq i} \delta(\mathbf{r}-\mathbf{r}_i)\delta(\mathbf{r}'-\mathbf{r}_j) \ . \tag{3.16}$$

Note that self-correlations have been explicitly excluded in (3.16). We now average (3.16) over the disorder, and then Fourier transform with respect to the variables $\mathbf{r}$ and $\mathbf{r}'$. This leads to

$$\int d^3r \int d^3r' e^{i\mathbf{q}\cdot\mathbf{r}} e^{i\mathbf{q}'\cdot\mathbf{r}'} n_2(\mathbf{r},\mathbf{r}') = \langle \hat{n}(\mathbf{q})\hat{n}(\mathbf{q}')\rangle - N\delta_{\mathbf{q}_\perp+\mathbf{q}'_\perp,0} f(q_z+q'_z)/t \ , \tag{3.17}$$

where n_2 is the average of the two-particle density operator in (3.16) and $\hat{n}(\mathbf{q})$ is defined in (3.5) (without the subscript m). The density in a finite slab of area A, thickness t, and containing N ions, is a product of the average density $n_0[=N/(At)]$ and a density profile function $f(z)$, which describes deviations in the average density at the boundaries, i.e.,

$$n(\mathbf{r})=n_0 f(z) \ , \tag{3.18}$$

and $f(q_z)$ in (3.17) is the Fourier transform of the density profile function. We will consider specific forms of f later in this section. From translational invariance and homogeneity of the two-particle density in the x-y plane (i.e., for a slab geometry) we have

$$n_2(\mathbf{r},\mathbf{r}')=n_2(|\mathbf{r}_\perp-\mathbf{r}'_\perp|,z,z') \ . \tag{3.19}$$

This shows that only the Fourier modes that satisfy $\mathbf{q}'_\perp=-\mathbf{q}_\perp$ in (3.17) are correlated. We next define the pair distribution function g in terms of the two- and one-particle densities, i.e.,

$$n_2(R,z,z')=n(R,z)n(R,z')g(R,z,z') \ , \tag{3.20}$$

where $R=|\mathbf{r}_\perp-\mathbf{r}'_\perp|$. Note that in an uncorrelated system g equals unity. By substituting (3.19) and (3.20) in (3.17) and carrying out a few simple manipulations, we obtain

$$\frac{1}{N}\langle n(q_\perp,q_z)n(-q_\perp,q'_z)\rangle - N\frac{f(q_z)f(q'_z)}{t^2}\delta_{q_\perp,0} = \frac{f(q_z+q'_z)}{t} + \frac{n_0}{t}\int dz \int dz' e^{iq_z z} e^{iq'_z z'} f(z)f(z') \int d^2R \, e^{-i\mathbf{q}'_\perp\cdot\mathbf{R}} h(R,z,z') \ , \tag{3.21}$$

where $h=g-1$ is the total correlation function. The left-hand side of (3.21) is taken as the definition of the structure factor in a slab geometry of finite extent in the z direction.

From (3.21) it is easy to see that in a system that is homogeneous in all three dimensions, for which $f(z)$ equals unity and $h(\mathbf{r},\mathbf{r}')=h(|\mathbf{r}-\mathbf{r}'|)$, the structure factor reduces to the usual definition,[15] i.e., $S=S^{3D}(q)$, where

$$S^{3D}(q)=1+n_0\int d^3r \, e^{i\mathbf{q}\cdot\mathbf{r}} h(r) \ . \tag{3.22}$$

The quantity in (3.22) is known analytically from the theory of liquids for hard-sphere pair potentials evaluated within the Percus-Yevick approximation.[32,33] This knowledge can be used to obtain an approximate structure factor of a thick slab (where we may continue to assume that the pair distribution function g is translationally invariant and homogeneous) but we incorporate the effects of the slab boundaries in the *one-particle density*. The density profile is assumed to be constant within a slab; since any variation at the boundaries is negligible for a thick slab, we take f to be

$$f(z)=\theta(z+t/2)-\theta(z-t/2)=\begin{cases}0, & |z|>t/2\\ 1, & |z|\leq t/2\end{cases} \ . \tag{3.23}$$

With these approximations we obtain the structure factor of a thick slab $S_>$ as

$$S_>(q_\perp,q_z,q'_z) = \frac{2}{\pi t}\int_{-\infty}^{\infty} dp \frac{\sin[(q_z-p)t/2]}{q_z-p}\frac{\sin[(q'_z+p)t/2]}{q'_z+p} \times S^{3D}[(q_\perp^2+p^2)^{1/2}] \ . \tag{3.24}$$

As the thick-slab limit is approached, the terms of the form $(\sin nx)/\pi x$ in (3.24) tend to δ functions. These can be approximated by a sequence of Gaussians and we obtain

$$S_> = \frac{t}{2} e^{-[(q_z+q'_z)t/2]^2} \int_0^\infty dp \, e^{-p^2t^2/2}[\alpha(p)+\alpha(-p)] \ , \tag{3.25}$$

where $\alpha(p)=S^{3D}\{[q_\perp^2+(p+\beta)^2]^{1/2}\}$ with $\beta=(q_z-q'_z)/2$. The integral in (3.25) can be easily evaluated in terms of gamma functions $\Gamma(z)$, by rescaling p by $1/t$ and then expanding about $1/t=0$, which gives

$$S_>(\mathbf{q}_\perp,q_z,q_z')=\frac{1}{\sqrt{2}}e^{-[(q_z+q_z')t/2]^2/2}\times\sum_{m=0}^{\infty}\frac{\alpha^{(2m)}(0)}{(2m)!}\frac{2^m}{t^{2m}}\Gamma(m+1/2)$$
$$=\delta_{q_z,q_z'}\left[S^{3D}(q)+\frac{1}{2t^2}\alpha^{(2)}(0)\right]+\cdots . \tag{3.26}$$

Equation (3.26) is taken as the structure factor in the thick-slab limit. The dependence on the packing fraction has been suppressed in this form. We next turn to the opposite thin-slab limit.

As mentioned previously, the structure factor of a three-dimensional (3D) homogeneous liquid in the thermodynamic limit, interacting via hard-sphere pair potentials is known analytically within the Percus-Yevick (PY) approximation.[32,33] No such equivalent is known so far in two dimensions. We have however observed, as a purely empirical matter, that by "scaling" this three-dimensional structure factor, we can obtain an accurate approximation to the structure factor for hard disks in two dimensions (2D). Scaling of the 3D function is performed according to the prescription

$$S_{2D}(x,y)=S_{3D}[((x/p)^q,(y/r)^s)] , \tag{3.27}$$

where $x\equiv q_\perp\sigma$ and the areal packing fraction $y=(N/A)\pi(\sigma/2)^2$, in terms of the hard-core diameter σ. The quality of this mapping has been checked against numerical solutions of the hard-disk structure factor within the PY approximation[34] and agrees to within 10% for the range of x shown in Fig. 2 for $y=0.38$ and 0.75. The parameters p, q, r, and s, are constants, *independent* of x and y, and are obtained by a least-squares fit of the scaled two-dimensional structure factor, the latter being determined numerically. Equation (3.27) is of sufficient accuracy for a description of the structure of an atomically thin slab of thickness $t\sim\sigma$.

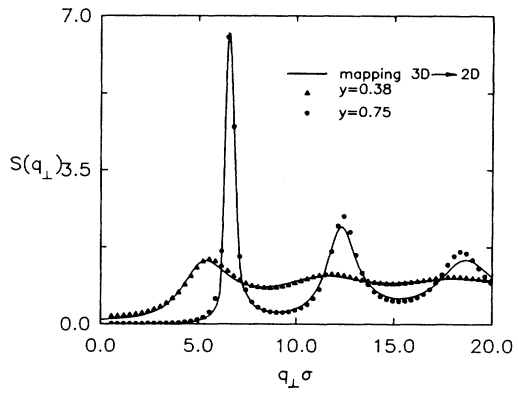

FIG. 2. Structure factor S for hard-disk pair potentials in two dimensions as obtained by a semi-empirical scaling of the corresponding three-dimensional hard-sphere structure factor known analytically in the Percus-Yevick (PY) approximation. A comparison of the scaled structure factor (solid lines) with the numerical solution of the PY equation for hard disks is shown for $y=0.38$ (triangles) and 0.75 (circles).

In a thin slab it is reasonable to assume that the dominant source of pair correlations is the *in-plane* contribution. This follows from the small extent of excursions in the z direction, and it allows us to write $h(R,z,z')\sim h(R)$ as a possible approximation. The effect of a finite boundary is again included in the prescription of the one-body density profile function which is taken as a Gaussian

$$f(z)=e^{-z^2/2\gamma^2} , \tag{3.28}$$

where γ is the root mean-square deviation of the centers of the particles from a plane. Using (3.28) in (3.21), we obtain an approximation to the structure factor of a thin slab ($S_<$) given by

$$S_<(q_\perp,q_z,q_z';\eta)=\frac{\sqrt{2\pi}\gamma}{t}e^{-(q_z+q_z')^2\gamma^2/4}+\frac{N}{N_{2D}}\frac{2\pi\gamma^2}{t^2}[S^{2D}(q_\perp;3\eta/2)-1]\times e^{-q_z^2\gamma^2/2}e^{-q_z'^2\gamma^2/2} . \tag{3.29}$$

In (3.29) the thickness t, which is otherwise not well determined when the density profile is diffuse, is defined to be $\sqrt{2\pi}\gamma$, and $N/N_{2D}=(t+\sigma)/\sigma$. Note that S^{2D} is the two-dimensional analog of (3.22) and is obtained by using (3.27). If the slab structure factor is required at a packing fraction $\eta=\frac{1}{6}\pi\sigma^3(N/V)$, the effective corresponding two-dimensional packing fraction $\eta_{2D}=\frac{1}{4}\pi\sigma^2(N/A)$ required to describe the correlations in a plane, or more appropriately in a slab of thickness σ, is given by $\eta_{2D}=\frac{3}{2}\eta$.

Equations (3.26) and (3.29) constitute the basic structural approximations describing a disordered interfacial region in two opposite limits. In the evaluation of the transition matrix elements, only the diagonal part, i.e., $q_z'=q_z$ of both $S_<$ and $S_>$ are required.

IV. RESULTS

We examine an interdiffusion model for a heterostructure with aluminum as the *host metal* containing an array of slabs of disordered tetravalent scatterers e.g., Si and *assumed embedded in the metallic environment.* As noted earlier this model does *not* imply a physical dissolution of the scatterers in the metallic host, which is known in the case of, say Al-Si to be small ($\sim 2\%$) in the *bulk* phase. However, on an atomic scale this model pertains to roughness scattering in interfacial regions over 2—3 atomic layers. It also describes scattering from grain boundaries formed between regions of dissimilar structural configurations. In our model aluminum is treated as a free-electron metal with a Fermi wave vector $k_Fa_0=0.93$ and the tetravalent ($Z=4$) scattering centers are described in the metallic host by an empty-core model for the electron-ion pseudopotential defined by

$$U(r)=\begin{cases}0, & r<R_c\\ -Ze^2/r, & r\geq R_c\end{cases} . \tag{4.1}$$

The Fourier transform of the ionic potential when screened by the Lindhard dielectric function $\epsilon_L(q)$ is

$$U(q)=-\frac{4\pi Ze^2}{q^2\epsilon_L(q)}\cos(qR_c)=-\tfrac{2}{3}\varepsilon_F\nu(q)(Z/n_{\rm el})\ , \qquad (4.2)$$

where $U(q)$ has been written in terms of a dimensionless potential $\nu(q)=\cos(qR_c)/[\pi k_F a_0(q/2k_F)^2+f(q/2k_F)]$ with a core radius[35] for silicon $R_c=0.74a_0$. In Eq. (4.2) $n_{\rm el}$ is the electronic density. The dielectric function is given by

$$\epsilon_L(q)=1+(\pi k_F a_0)^{-1}(2k_F/q)^2 f(q/2k_F)\ , \qquad (4.3)$$

where the Lindhard function f is defined as

$$f(x)=\frac{1}{2}+\frac{1-x^2}{4x}\ln\left|\frac{1+x}{1-x}\right|\ . \qquad (4.4)$$

The thermopower, as shown in (C10) and also in (4.7), requires, in addition, the derivative of the pseudopotential with respect to the energy of the electron. As is well known, the ground-state Lindhard dielectric function ϵ_L has a weak logarithmic singularity at $q=2k_F$. This singularity is known to give rise to Friedel oscillations in the ion-ion potential at large distances and is also responsible for Kohn anomalies seen in phonon spectra. (However, at finite temperatures, the singularity in ϵ_L is smoothed out.) It has been shown by Pettifor and Ward[36] that the function f in (4.4) can be replaced by a rational function with the correct high- and low-q behavior, which thereby avoids the problem arising from the singularity. We use this form for f in the evaluation of the thermopower.

The structural anisotropy present in the heterostructure is introduced via positional correlations between silicon scattering centers within a slab. For a slab of thickness t and concentration n_0 of scattering centers the correlation function is determined as described in Sec. III. The structure factor of a thin slab is contained in (3.27) and (3.29) and that of a thick slab in (3.26). It is assumed that the interimpurity potential can be described by a hard core of diameter $\sigma=5.0a_0$ (Ref. 32) in terms of which a dimensionless parameter $\eta=\frac{1}{6}\pi\sigma^3 n_0$ is then defined to characterize the concentration of scatterers.

The matrix elements of the averaged transition probability $\langle W\rangle$ in (3.15), essentially proportional to the square of the electron-ion pseudopotential and the structure factor, are obtained by a three-dimensional numerical integration [see (B7) and (B11)]. From this the components of the resistivity tensor can be directly obtained and are given by

$$\rho_{zz}=\left[\rho_{\rm at}\frac{3\pi^5Z^2}{(k_Fa_0)^4}(n_0a_0^3)\frac{t}{d}\right]\frac{1}{4\pi I^{-1}(1,0;1,0)}\ . \qquad (4.5)$$

Similarly, ρ_{xx} is found to be inversely proportional to $I^{-1}(1,1;1,-1)$ with the same prefactor as in (4.5). As seen from (B6), I is proportional to the matrix elements of transition probability W. In (4.5), $\rho_{\rm at}$ is the atomic unit of resistivity ($a_0\hbar/e^2\equiv 21.7\ \mu\Omega\,{\rm cm}$) and d is the modulation period of the superlattice structure. In the isotropic limit, the transition rate depends only on the angle γ between the vectors $\mathbf{k}$ and $\mathbf{k}'$ and (4.5) reduces to [see (B14)]

$$\rho=\left[\rho_{\rm at}(n_0a_0^3)\frac{3\pi^5Z^2}{(k_Fa_0)^4}\right]\int_{-1}^{1}d\cos\gamma\,\nu^2(q)S(q)\times(1-\cos\gamma)\ , \qquad (4.6)$$

where $\nu(q)$ is introduced in (4.2) and $q=2k_F\sin(\gamma/2)$ in (4.6). The isotropic limit obtained in (4.6) agrees with the expression for the Ziman resistivity in liquid metals.[25] The thermopower for the superlattice geometry is obtained by a generalization of the isotropic case outlined in Appendix C. Using the definition in (2.10), we obtain

$$\xi_{\mu\mu}=1-2\pi\left[\varepsilon M_{ij}\frac{1}{(4\pi I^{-1})_{ij}}\right]_{\varepsilon=\varepsilon_F}\ , \qquad (4.7)$$

where $(i;j)=(1,0;1,0)$ for the thermopower component ξ_{zz} and $(i;j)=(1,1;1,-1)$ for ξ_{xx} and

$$M_{ij}=\left[I^{-1}\frac{dI}{d\varepsilon}I^{-1}\right]_{ij}\ . \qquad (4.8)$$

The thermopower $\xi_{\mu\mu}$, as seen in Eq. (2.10), is measured in units of $-\pi^2k_B^2T/(3\,|\,e\,|\,\varepsilon_F)$ which equals

$$(-2.44\times10^{-2})\ (\mu V/{\rm K})[T({\rm K})/\varepsilon_F({\rm eV})]\ .$$

In Fig. 3 are shown the out-of-plane component ρ_{zz} and the in-plane component ρ_{xx} for an atomically thin slab, as a function of η up to a maximum of 0.6, which is close to the dense random packing limit[37] at 0.637. At low packing fractions, the resistivity increases linearly with η. This behavior is characteristic of scattering from a random distribution of uncorrelated scattering centers. At

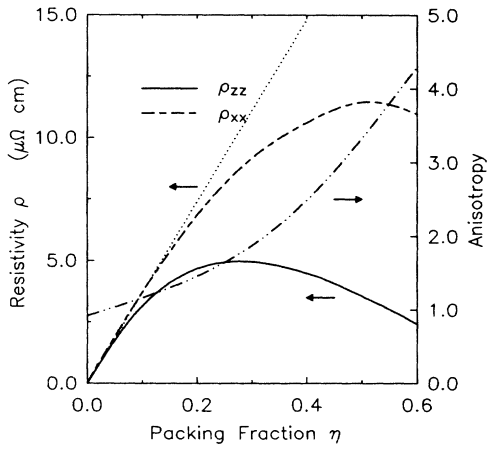

FIG. 3. Resistivity components for metallic heterostructure with slabs simulating disordered interfacial regions. Shown are the in-plane ρ_{xx} and out-of-plane resistivity ρ_{zz} and the anisotropy parameter ρ_{xx}/ρ_{zz} vs η, the packing fraction of impurity ions. The slab thickness is $t=5a_0$ and the modulation period is $d=100a_0$. For a uniform distribution of ions in the slab the resistivity components are equal and their behavior is indicated by the dotted line. Note the different scales for the resistivity and the anisotropy.

higher η, the resistivity components increase more slowly; ρ_{zz}, in fact, reaches a maximum at $\eta \sim 0.3$. These trends can be understood as follows: For a nearly uniform distribution of scattering centers, the Fourier components in the structure factor are of almost equal strength and momentum transfer over a wide range from 0 to $2k_F$ is effective in the electron-impurity scattering process. The initial rise in ρ with η is, therefore, mainly a consequence of the increase in the density of scattering centers. However, further increase in ion density results in local structural organization, which is reflected in a very strong Fourier component in $S(q)$. The scattering of electrons is now dominated by a very narrow band width (in momentum space) around $q \sim 2\pi/a$ where a is the average distance between particles. This leads to a reduction in the resistivity. The anisotropy in the transport coefficients which is taken as the ratio between ρ_{xx} and ρ_{zz}, progressively increases with η. The resistivity components, which are essentially equal at low η, differ by a factor of almost 5 for $\eta \sim 0.6$.

The components of the thermopower ξ_{zz} and ξ_{xx} [in dimensionless units, see (4.7) and (2.10)] are shown in Fig. 4 for an atomically thin slab. The thermopower essentially probes the change in the "resistivity" with the energy of the electrons. Our results suggest that the thermopower component along the superlattice axis is more sensitive to the disorder than the in-plane component. In addition, an application of the variational principle yields the expansion coefficients of the distribution function in Eq. (B3), from which a scattering time $\tau(\mathbf{k})$ can be extracted and is defined by $\Phi(\mathbf{k}) = e\mathbf{E}\cdot\mathbf{v}(\mathbf{k})\tau(\mathbf{k})$. Note that as discussed in Sec. II, the scattering time is clearly a functional of the distribution function Φ. This is shown on a polar plot in Fig. 5 for an electric field applied along the superlattice axis. Pronounced deviations from isotropic behavior in the scattering time can be seen at high densities.

In the thick-slab limit, we find that the deviations of $O(1/t^2)$ in the transport coefficient arising from finite-size corrections in the structure factor (3.26) are negligible, as expected. The isotropic limit is therefore a good description of the thick slab and the resistivity and thermopower in this limit are shown in Figs. 10 and 11 as a function of η.

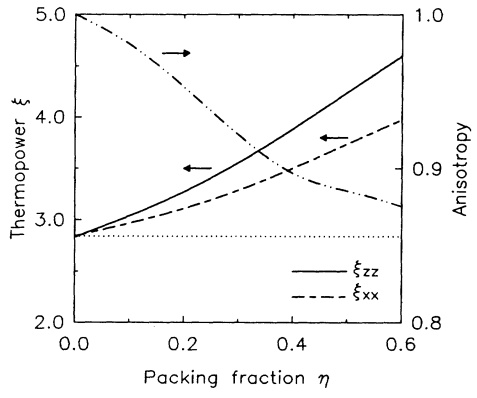

FIG. 4. Thermopower components (dimensionless), in-plane ξ_{xx} and out-of-plane ξ_{zz} and the anisotropy parameter ξ_{xx}/ξ_{zz} vs η, the packing fraction. The slab thickness is $t = 5a_0$ and the modulation period is $d = 100a_0$. In the absence of positional correlations in a slab, the thermopower components are equal and independent of η, as shown by the dotted line.

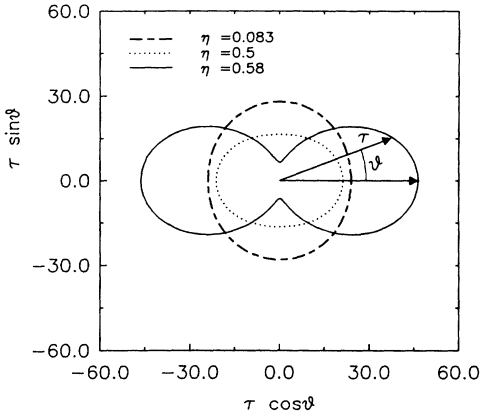

FIG. 5. Scattering time τ on a polar plot for an electric field applied along the superlattice axis. The scattering rate, in this case, depends only on the polar angle $-\pi/2 \le \theta \le \pi/2$ measured with respect to the superlattice axis and is symmetric for back-scattering angles. The curves are parametrized by the packing fraction within a slab. The slab thickness is $t = 5a_0$ and the modulation period is $d = 100a_0$. Marked deviations from isotropic behavior become apparent at high η when correlations are important.

The behavior of the transport coefficients as a function of t is known from our calculation in two regimes: for slabs a few atomic layers thick, and for thick slabs in which t is greater than the electron mean free path. It is possible to interpolate between these limits; however, it must be noted that in our model we have assumed that the modulation period is much greater than the thickness of a slab; therefore, such an interpolation is relevant only in so far as it does not violate this assumption. In Fig. 6 the resistivity components ρ_{zz} and ρ_{xx}, calculated in the thin-slab limit by using the structure factor in (3.29), are plotted as a function of t. Their behavior is almost linear with a slope of 3.6 and 1.5 for the z and x components, respectively. Using the resistivity, an effective mean free path l_{eff} can be defined in the system which is itself a function of t. With further increase in t, as l_{eff} becomes less than the thickness of a slab, both the resistivity components start approaching a slope of $\sim \rho_{\text{iso}}/d$ where ρ_{iso} is the resistivity in a bulk three-dimensional system of aluminum metal containing the same density of scattering ions as in the slabs. Finally, as the thickness of a slab approaches the modulation period, the resistivity saturates at the value of ρ_{iso} and consequently, the anisotropy parameter ρ_{xx}/ρ_{zz} approaches unity. The inset in Fig. 6 shows the crossover from the thin-to the thick-slab regimes (obtained by a cubic spline interpolation technique) as l_{eff} becomes of the order of t. The components of the thermopower as a function of t are shown in Fig. 7.

For a fixed slab of thickness t and density of atoms n_0, both the in-plane and out-of-plane resistivity components

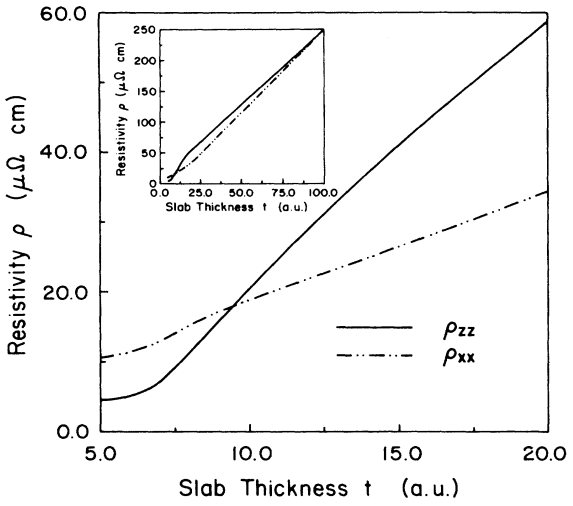

FIG. 6. Resistivity components in the thin-slab regime. Out-of-plane component ρ_{zz} and the in-plane component ρ_{xx} vs t, the thickness of a slab. The packing fraction within a slab is $\eta=0.5$ and the modulation period is $d=100a_0$. The inset shows a crossover from the thin-slab to the thick-slab limit as t approaches the effective mean free path of the electrons. A cubic spline interpolation of the resistivity components is performed between these two limits.

vary inversely with the spacing between slabs d, as seen from Eq. (4.5). This behavior is a signature of a mean free path that is limited by boundary scattering. More interestingly, as the distance between slabs approaches the thickness of a slab, both the resistivity components become equal and together saturate at the value $\rho_{\rm iso}$ (see Fig. 8).

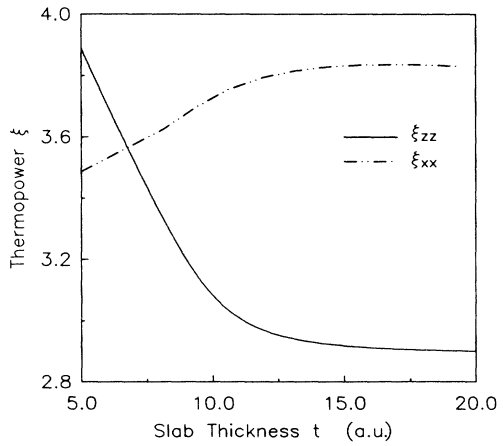

FIG. 7. Out-of-plane thermopower component ξ_{zz} and the in-plane thermopower component ξ_{xx} vs t, the thickness of a slab in the thin-slab regime. The fixed parameters are the packing fraction within a slab $\eta=0.5$ and the modulation period $d=100a_0$.

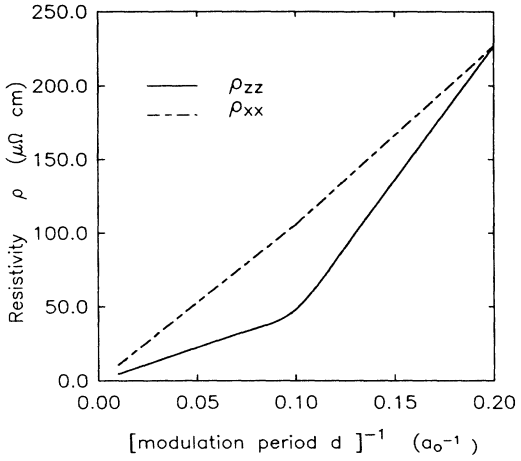

FIG. 8. Resistivity components, in-plane ρ_{xx}, and out-of-plane ρ_{zz} vs $1/d$, the inverse of the modulation period. This is shown for a fixed packing fraction $\eta=0.5$ and a slab thickness $t=5a_0$. As d approaches $\sim 15a_0$ a crossover behavior is seen (more prominent in ρ_{zz}) and the resistivity components approach the isotropic limit.

V. DISCUSSION AND CONCLUSION

Our results illustrate the effect the structure of an interface, incorporated via positional correlations between ions at the interface, has on the transport properties of the superlattice. Deviations from linear dependence of both the in-plane and out-of-plane resistivity components ρ_{xx} and ρ_{zz}, respectively, as a function of the degree of disorder n_0 (or η in our calculation) are predicted, where z is taken to be along the superlattice axis (Fig. 3). In fact, at packing fractions typical of solids, the resistivity can even decrease with increasing n_0. Correlations also induce *anisotropy* between the in-plane and out-of-plane transport coefficients; ρ_{xx} can become almost five times higher than ρ_{zz}. The thermopower is a more *sensitive* probe of the disorder compared to the resistivity (since it involves a derivative of the "resistivity"). We find that the out-of-plane component can become almost 25–30% larger than the in-plane component as n_0 is increased (Fig. 4).

The effect of the interfacial structure can also be seen in the dependence of the transport coefficients on the thickness of the disordered region t. For $t\sim 3$–4 atomic layers, ρ_{xx} is not very sensitive to the correlations along the z direction. On the other hand, ρ_{zz}, which is initially lower than ρ_{xx} for an atomically thin interface, rises much more rapidly, with a slope almost twice as large as for ρ_{xx} (Fig. 6). Once again, the out-of-plane component of the thermopower "sees" a more pronounced effect of the correlations along the z direction compared to the in-plane component; ξ_{zz} decreases by as much as 25% as the thickness of the interface is increased from 1 to 4 atomic layers, whereas ξ_{xx} shows only a 5% increase (Fig. 7).

Besides the structure of the interface, the choice of the *pseudopotential* describing the ions at the interface also has a marked effect on the resistivity and the thermopower. In our calculation, the pseudopotential of the

scattering center has been characterized by the empty-core radius R_c [see (4.1)] and is shown in Fig. 9 for $R_c = 0.67, 0.74, 0.8$ in atomic units. In Figs. 10 and 11 the transport coefficients are shown for the isotropic system consisting of bulk aluminum with scattering centers described by the above three different values of R_c. Similar calculations for the superlattice geometry also depict this degree of sensitivity of the transport coefficients on the choice of the pseudopotential.

The features just described have so far not been explored experimentally. However, it should be possible to study the predictions indicated above, since t and n_0 can both be measured in x-ray diffraction experiments. The thickness of the interface can also be monitored by depth profiling techniques such as Rutherford backscattering. In addition, the disorder at an interface can be increased by ion bombardment or decreased by annealing. Another interesting technique that can probe the thickness dependence of the resistivity is the pulsed laser and electron beam annealing of silicon.[38] This experiment has so far used conductance measurements to determine the thickness t of the molten silicon layer. The assumption made is a linear dependence of the conductance on an apparent melt depth and on the resistivity of molten silicon ($\rho_{\text{liquid}} \sim 80\ \mu\Omega$ cm). This implies that the resistivity of the molten layer, as a function of the thickness t is a constant and finite-size effects are not considered. This would appear to be a reasonable approximation for t of the order of a few hundred angstroms (as is the case in these experiments), and is corroborated by our calculation of the structure factor of a thick slab. (We find that the $1/t^2$ corrections to the resistivity of a bulk metal are indeed negligible for $t \sim 100$ Å.) However, for smaller thickness, of order 10 Å, finite-size effects calculated for the replicated slab model show that the resistivity is no longer independent of t (see Fig. 6); the estimation of t from conductance measurements alone is then not a straightforward matter. Nevertheless, if the laser annealing experiment is combined with interferometric techniques to obtain the thickness of the molten layer, then conductance measurements can once again be used to measure the finite-size corrections to the resistivity.

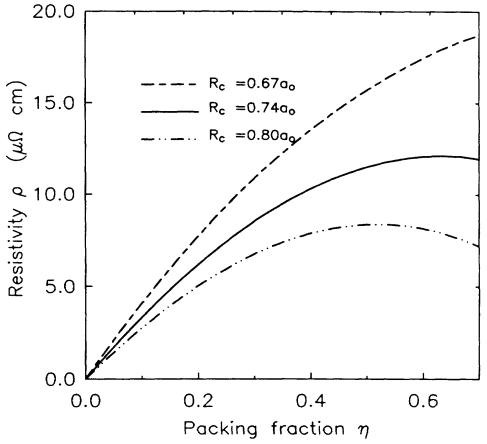

FIG. 10. Resistivity of an isotropic system in three-dimensions (Al host metal containing silicon impurities) as a function of the packing fraction η for different core radii R_c. A 10% variation in R_c can lead to almost 50% change in the resistivity. This reveals the sensitivity of the transport coefficients to the choice of the pseudopotential.

Although the transport properties of a superlattice as a function of the interface parameters have not been explored so far, there are measurements of the in-plane resistivity ρ_{xx} as a function of the modulation period d which show an inverse dependence on d. Qualitatively,

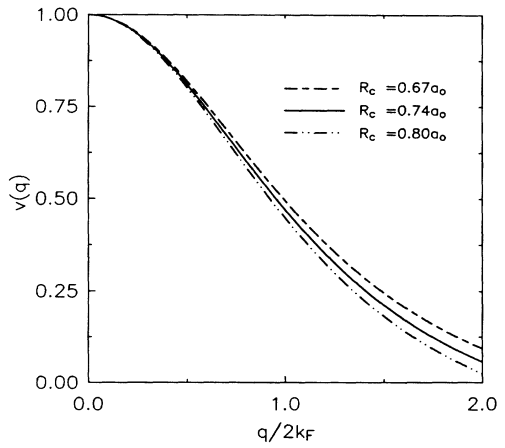

FIG. 9. Scattering ion empty-core pseudopotential screened by the Lindhard dielectric function shown in units of $-\frac{2}{3}\varepsilon_F$. A core radius $R_c = 0.74a_0$ is used in the calculations to describe $v(q)$ for silicon. Shown is the deviation in $v(q)$ for a 10% variation in R_c.

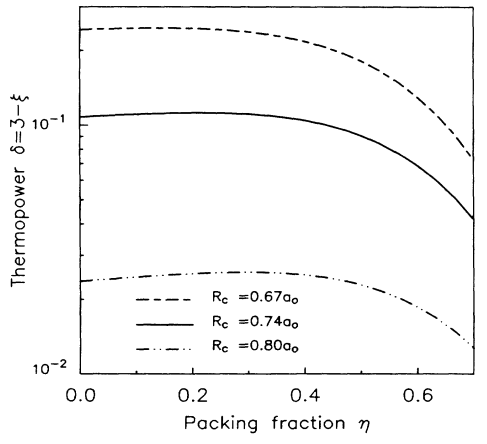

FIG. 11. Thermopower ξ for an isotropic system as a function of η for varying core radii R_c. Shown is the deviation of ξ from the pseudopotential-independent part on a logarithmic scale. δ is even more sensitive to the choice of the pseudopotential than the resistivity and can vary by a factor of 3 for a 10% change in R_c.

this behavior can be easily understood as arising from a mean free path that is limited by boundary scattering at the layers. To date, this behavior has been accounted for by the finite-size-effect theory of Fuchs[11] and Sondheimer[12] and of Mayadas and Shatzkes.[39] These theories describe the scattering effects of an interface via a phenomenological specularity parameter p. But, their applicability to superlattice geometries is questionable since they have been originally derived for metallic films which do not allow for transmission at the interfaces.

As can be seen in Fig. 8, our calculation also gives an inverse dependence of the in-plane resistivity on d. However, before a meaningful comparison of the slope of the ρ_{xx} versus $1/d$ data with our theory can be made, one other physically important feature must be taken into account. Various metallic superlattices, for modulation period d less than ~ 10 Å, show a tendency to saturate close to the Ioffe-Regel limit,[40] which is attained when the effective mean free path becomes of the order of the inverse Fermi wave vector. In Nb-Cu and Nb-Ti superlattices,[9,10] the saturation resistivity is found to be 160 and 115 $\mu\Omega$ cm, respectively. From our model calculation for an array of disordered interfaces, it is seen in Fig. 8 that as the layer periodicity approaches the thickness of the disordered interface, the resistivity saturates around 220 $\mu\Omega$ cm. The difference in the value of the saturation resistivity seen in experiments on metallic superlattices and the model calculation is attributable to two factors. In the limit of small modulation periods, the system of alternating A and B layers can be regarded as a bulk A-B alloy. As can be seen from (4.6) and (B14), the resistivity of a three-dimensional isotropic system is essentially proportional to an integral, over the momentum transferred, of the square of the pseudopotential times a structure factor. For typical solid densities or packing fractions in the interface, the integral is dominated by the region under the first peak in the structure factor. Thus, the factors influencing the saturation resistivity are the density of scattering centers (determining the height and peak position of the structure factor) and the nature of elements constituting the interface (determining the pseudopotential). To compare the slope of the ρ_{xx} versus $1/d$ data with our theory we first scale out the differences in the pseudopotential by measuring ρ_{xx} in units of the saturation resistivity. We then find that the calculated slope of the scaled ρ_{xx} versus $1/d$ differs from the slope in Nb-Ti and Nb-Cu by a factor of 1.8 and 2.5, respectively. Since the pseudopotential is scaled out only on average, this agreement is satisfactory.

As mentioned is Sec. III, the replicated slab model also has bearing on the transport properties of a single junction. We define the specific contact resistance R_c to be a product of the out-of-plane resistivity ρ_{zz} and the layer periodicity d. Similarly, the specific boundary resistance R_B is defined as a product of ρ_{xx} and d. The calculation depicted in Fig. 3 for a slab thickness of $\sim 5a_0$ and $d \sim 100a_0$ shows that ρ_{zz} peaks at a packing fraction $\eta \sim 0.2$. This corresponds to $R_c \sim 2.5$ pΩ cm^2; the boundary resistance at this packing fraction is higher by a factor of 2. If we consider a typical cross sectional area of 1 square micrometer, the contact resistance per atom denoted by $r_c = R_c/(NA)$ is ~ 40 pΩ. It is important to note that the specific contact resistance calculated above for an Al-Si junction with silicon embedded in a metallic host is about six orders of magnitude lower than the *tunneling* characteristics in an ohmic contact between aluminum and heavily doped n^+ silicon. This is as expected because the transport process in the latter case is dominated by a barrier penetrating between Al and Si. Our results for the contact resistance of a single junction do however corroborate very well with data on the resistance of *single grain* boundaries in aluminum.[41] Nakamichi and Kino measure specific grain-boundary resistances of order a few pΩ cm^2 as a function of rotation angle (between regions on either side of the grain boundary).

We have so far emphasized the effect of the structure of an interface on the transport properties of the system. Having understood this correlation, it then becomes possible in principle to invert the information in the transport coefficients and extract the structural features from it, *provided* the pseudopotential is known. Thus, by such characterization, transport measurements can become a viable tool for interpreting structure. For example, as in Fig. 6, a family of curves parametrized by the density of scattering centers n_0 and showing the resistivity as a function of t can be obtained. Similarly, a family of curves for the thermopower components as in Fig. 7 can also be determined. With these two sets of data, both the thickness t and n_0 can be read off directly for a measured ρ and ξ. By measuring both the in-plane and out-of-plane components of the resistivity and thermopower, the structural parameters t and n_0 can be checked independently. The microscopic model of interdiffusion in a heterostructure studied in this paper can be further generalized to include scattering by two species within a slab. In addition, by superimposing a density profile for the components of the interface, the model can also give a microscopic description of transport in a graded interface. With reference to the experiments on grain-boundary resistance ρ_{GB} in metals, extension of our calculations on the replicated slab model strongly suggests the possibility of establishing a correlation between ρ_{GB} and the structure. Furthermore, the intrinsic ρ_{GB} are so small (of order $p\Omega$ cm^2) that the experiments are extremely sensitive to factors such as the purity of metals, etc. Therefore, theoretical estimates of this kind may play a useful role not only to ascertain the quality of samples used in the experiments but also in a more fundamental way to test and predict the structures of grain boundaries.

ACKNOWLEDGMENTS

We would like to especially thank Professor F. Lado for providing us with his numerical solution of the Percus-Yevick structure factor for hard disks and Dr. J. Zollweg for Monte Carlo simulation data for the radial distribution function of hard disks at high packing fractions. Thanks are also due to Professor S. Sass and Professor M. Thompson for useful discussions on the grain-boundary resistance in metals and the laser annealing experiments in silicon. This work has been supported by the Semiconductor Research Corporation program on Microscience

and Technology at Cornell University, under Contract No. 82-11-001.

APPENDIX A

We show that for an anisotropic collision kernel W it is not possible to obtain a straightforward solution of the Boltzmann equation within a relaxation-time approximation. We begin by expanding W in a double harmonic series given by

$$W_{\mathbf{k}\mathbf{k}'}=\delta(\varepsilon_{\mathbf{k}}-\varepsilon_{\mathbf{k}'})\sum_{l,m}\sum_{l',m'}\omega[l,m;l',m']Y_{lm}(\Omega)Y_{l'm'}(\Omega')\ , \tag{A1}$$

where Ω and Ω' are the angles of $\mathbf{k}$ and $\mathbf{k}'$, respectively, with respect to some reference axis, and ω are the expansion coefficients of W. The distribution function is once again expanded in spherical harmonics as in (2.4). After some algebra it can be shown that if a scattering time τ is defined in terms of the expansion coefficients of the collision kernel by

$$\frac{1}{\tau[l,m;l',m']}=\Omega\frac{N(k)}{4\pi}\left[\sum_n\sqrt{2n+1}\,\omega[n,m-m';0,0]C_n(l,m;l',m')-(-1)^{m'}\omega[l,m;l',-m']\right], \tag{A2}$$

where Ω is the volume of the system (not to be confused with solid angles) and $C_n(l,m;l',m')$ is the Clebsh-Gordon coefficient given by

$$C_n(l,m;l',m')=\left[\frac{4\pi}{2n+1}\right]^{1/2}\langle Y_{lm}\mid Y_{n,m-m'}\mid Y_{l'm'}\rangle\ , \tag{A3}$$

then (2.2) reduces to

$$\left[\frac{\partial f_{lm}}{\partial t}\right]_{\text{coll}}=-\sum_{l'm'}\frac{f_{l'm'}}{\tau[l,m;l',m']}\ . \tag{A4}$$

Equation (A4) shows that the relaxation of a particular mode, labeled by (l,m), is coupled to all other modes and therefore the relaxation-time approximation is not justified. If we now define an effective rate by

$$\frac{1}{\tau_{lm}^{\text{eff}}}=\frac{1}{\tau_{lm}}\left[1+\sum_{\{l'm'\}\neq\{lm\}}\frac{f_{l'm'}}{f_{lm}}\frac{\tau_{lm}}{\tau[l,m;l',m']}\right], \tag{A5}$$

where $\tau_{lm}=\tau[l,m;l,m]$, then (A4) can be written in a form suggestive of the relaxation-time approximation as

$$\left[\frac{\partial f_{lm}}{\partial t}\right]_{\text{coll}}=-\frac{f_{lm}}{\tau_{lm}^{\text{eff}}[f_{lm}]}\ . \tag{A6}$$

However, note that this has been possible only at the cost of making the effective relaxation rate a functional of the distribution function.

Another approach, which leads to the same conclusion, is to start with the assumption that the nonequilibrium function does indeed relax to equilibrium with a time constant $t(\mathbf{k})$ which is a function of momentum $\mathbf{k}$. The right-hand side of (2.2) can then be written as

$$\left[\frac{\partial g(\mathbf{k})}{\partial t}\right]_{\text{coll}}=-\frac{g(\mathbf{k})-g^0(\varepsilon_{\mathbf{k}})}{t(\mathbf{k})}\ . \tag{A7}$$

It is convenient to expand the distribution function and relaxation rate in spherical harmonics with expansion coefficients f_{lm} and $1/t_{lm}$, respectively, as follows:

$$g(\mathbf{k})=g^0(\varepsilon_{\mathbf{k}})+\sum_{l,m}f_{lm}(\varepsilon_{\mathbf{k}})Y_{lm}(\Omega) \tag{A8}$$

and

$$\frac{1}{t(\mathbf{k})}=\sum_{l,m}\frac{1}{t_{lm}}Y_{lm}(\Omega)\ . \tag{A9}$$

If the expansion coefficients of the relaxation rate could be obtained by solving (2.2) and were indeed found to be independent of the distribution function, the relaxation-time approximation would then be valid. However, by substituting (A1), (A8), and (A9) in (A7) and in (2.2), we obtain

$$\sum_n\left[\frac{2n+1}{4\pi}\right]^{1/2}\frac{C_n(l,m;l',m')}{t_{n,m-m'}}=\frac{1}{\tau[l,m;l',m']}\ , \tag{A10}$$

where τ and C_n are defined in (A2) and (A3), respectively. Equation (A10) shows that it is not possible to extract the individual coefficients t_{lm}, if the relaxation time approximation is assumed; instead, only a constraint on the sum of t_{lm} is obtained.

APPENDIX B

In this section some details on a variational solution of the Boltzmann equation, to obtain the components of the resistivity tensor, are provided. Expressions for the transport coefficients pertaining to the replicated slab model introduced earlier are also obtained. The trial function $\Phi(\mathbf{k})$ in (2.7) can be expanded in spherical harmonic functions

$$\Phi_{\hat{n}}(\mathbf{k})=\sum_{l,m}^{(N)}\eta_{lm}^{\hat{n}}(\mid\mathbf{k}\mid)Y_{lm}(\Omega)\ , \tag{B1}$$

where $\hat{n}$ denotes the direction of the externally applied field. Equation (B1) is then substituted in the expression for the variational function ρ^{trial} defined in (2.7). By varying the expansion coefficients η_{lm}, an approximate minimum of ρ^{trial} is obtained, given by

$$\rho\leq\rho^{\text{trial}}(N)=\frac{1}{2}\left[\sum_{l,m}\sum_{l',m'}(J_{\hat{n}})_{l,m}W^{-1}(lm;l'm')(J_{\hat{n}})_{l'm'}\right]. \tag{B2}$$

Since a finite expansion set with N basis functions is used in (B1), only an *approximate* minimum of the variational function is found; however, as N increases, a sequence of decreasing upper bounds on ρ is found that eventually converge to the true answer. The expansion coefficients are given by

$$\eta_{lm}^{\hat{n}} = \sum_{l',m'} W^{-1}(lm;l'm')(J_{\hat{n}})_{l'm'} , \tag{B3}$$

where

$$(J_{\hat{n}})_{lm} = \int \frac{d^3k}{4\pi^3} e v_{\hat{n}}(\mathbf{k}) Y_{lm}(\Omega) \frac{-\partial g_{\mathbf{k}}^0}{\partial \varepsilon_{\mathbf{k}}} \tag{B4}$$

and

$$W(lm;l'm') = \int \frac{d^3k}{4\pi^3} \int \frac{d^3k'}{4\pi^3} [Y_{lm}(\Omega) - Y_{lm}(\Omega')] W_{\mathbf{kk}'} \times [Y_{l'm'}(\Omega) - Y_{l'm'}(\Omega')] . \tag{B5}$$

The above formalism is applied to the replicated slab model described in Sec. III. It consists of an array of M slabs in a total volume Ω, each slab containing N scattering centers for which the transition probability $W_{\mathbf{kk}'}$ is defined in (3.15). At zero temperature and for elastic scattering, the integrations over $|\mathbf{k}|$ and $|\mathbf{k}'|$ are straightforward, and for a metal with an isotropic dispersion relation, which is the case being considered in this paper, (B5) reduces to

$$W(lm;l'm') = \frac{2\pi}{\hbar} \frac{NM}{\Omega} \left[\frac{N(0)}{4\pi} \right]^2 \left[\frac{4\pi Z e^2}{k_{\mathrm{TF}}^2} \right]^2 I(lm;l'm') , \tag{B6}$$

where $N(0)$ is the density of states at the Fermi energy, Z is the valence of the scattering center, and k_{TF} is the Thomas-Fermi screening wave vector.

In (B6) I is given by

$$I(lm,l',m') = \int d\Omega \int d\Omega' [Y_{lm}(\Omega) - Y_{lm}(\Omega')] K(\Omega,\Omega') \times [Y_{l'm'}(\Omega) - Y_{l'm'}(\Omega')] . \tag{B7}$$

The dimensionless kernel K is a product of the square of the ion potential $v(q)$ defined in (4.2) and the structure factor given by

$$K(\varepsilon_F,\Omega,\Omega') = [\,|v(q)|^2 S(\mathbf{q})]_{\varepsilon=\varepsilon_F} , \tag{B8}$$

where $\mathbf{q}=\mathbf{k}'-\mathbf{k}$ and the right-hand side of (B8) is evaluated on the Fermi energy shell. The four-dimensional integration in (B7) is reduced to a three-dimensional integration by exploiting the symmetry properties satisfied by the kernel. To elaborate on this point, the kernel is expanded in a double harmonic series

$$K(\Omega,\Omega') = \sum_{l,m} \sum_{l'm'} \Gamma_{lm}^{l'm'} Y_{lm}(\Omega) Y_{l'm'}(\Omega') , \tag{B9}$$

with expansion coefficients

$$\Gamma_{lm}^{l'm'} = \int d\Omega \int d\Omega' \, Y_{lm}^*(\Omega) Y_{lm}^*(\Omega') K(\Omega,\Omega') . \tag{B10}$$

It can be easily verified that $K(\Omega,\Omega')=K(\Omega',\Omega)$ and $K(\phi,\phi')=K(\phi-\phi')$ where ϕ is an azimuthal angle. These relations imply that

$$\Gamma_{lm}^{l'm'} = \Gamma_{l'm}^{lm'} = \Gamma_{lm'}^{l'm} = \Gamma_{lm}^{l'-m} \delta_{m+m',0} .$$

Therefore the integral in (B7) simplifies to

$$\Gamma_{lm}^{l'-m} = 2\pi c_l^m c_{l'}^{-m} d_{l'}^m \int_{-1}^{1} d\cos\theta \int_{-1}^{1} d\cos\theta' \, P_l^m(\cos\theta) P_{l'}^m(\cos\theta') \int_0^{2\pi} d\tilde{\phi} \cos(m\tilde{\phi}) K(\theta,\theta',\tilde{\phi}) , \tag{B11}$$

where d_l^m and c_l^m are defined by

$$\begin{aligned} Y_{lm}(\theta,\phi) &= c_l^m P_l^m(\cos\theta) e^{im\phi} , \\ P_l^{-m}(\cos\theta) &= d_l^m P_l^m(\cos\theta) . \end{aligned} \tag{B12}$$

By substituting (B9) and (B11) in (B7) and using standard properties of spherical harmonics, we obtain

$$I(lm;l'-m) = 2(-1)^m \sum_n \sqrt{2n+1}\, \Gamma_{n,0}^{0,0} C_n(l,-m;l',-m) - 2\Gamma_{lm}^{l'-m} , \tag{B13}$$

where C_n is defined in (A3).

For an electric field applied along the z direction, substitution of (B4)–(B6) in (B2) yields ρ_{zz} which is inversely proportional to $I^{-1}(1,0;1,0)$. Similarly, for an electric field along the x direction, ρ_{xx} is found to be inversely proportional to $I^{-1}(1,1;1,-1)$. See (4.5) for the exact expression of the resistivity components. In our calculation we retain terms up to $l=3$ in the expansion of the trial function in (B1), I is then obtained by a three-dimensional integration which is evaluated numerically and finally a 15×15 matrix is inverted to obtain the inverse of matrix I. As shown above only two elements of I^{-1} are required to obtain the transport coefficients.

The isotropic limit

In the isotropic limit, the scattering kernel K depends only on the angle γ between the vectors $\mathbf{k}$ and $\mathbf{k}'$. Using the addition theorem for spherical harmonics, it can then be shown that the only nonzero terms in (B13) are those for which $l=l'$ and $m=0$, i.e.,

$$\begin{aligned} I(l) &= I(l,m;l',-m)\delta_{l,l'}\delta_{m,0} \\ &= 4\pi \int_{-1}^{1} d\cos\gamma \, K(\gamma)[1-P_l(\cos\gamma)] . \end{aligned} \tag{B14}$$

The resistivity components turn out to be equal, as would indeed be expected in the isotropic limit and are proportional to $I(1)$, which agrees with Ziman's expression for the resistivity of liquid metals.[25]

APPENDIX C

We present here the thermopower in the isotropic case to bring out the essential features. For the superlattice

geometry, the anisotropic case can be obtained by a straightforward generalization and the results are shown in (4.7) and (4.8).

In the entire discussion that follows, the electrons are assumed to satisfy an isotropic dispersion relation. The conductivity function when evaluated on an arbitrary energy shell leads to

$$\sigma(\varepsilon)=e^2\int\frac{d^3k}{4\pi^3}(\mathbf{v}_\mathbf{k}\cdot\hat{\mathbf{n}})^2\tau(\varepsilon_\mathbf{k})\delta(\varepsilon_\mathbf{k}-\varepsilon)\ , \tag{C1}$$

where $\hat{\mathbf{n}}$ is a unit vector in the direction of an externally applied uniform field. The angular integrals in (C1) can be easily carried out since the scattering time τ is a function of energy only. We obtain

$$\sigma(\varepsilon)=\frac{2e^2}{3m}\int d\varepsilon_\mathbf{k}h(\varepsilon_\mathbf{k})\delta(\varepsilon_\mathbf{k}-\varepsilon)\ , \tag{C2}$$

where $h(\varepsilon)=\varepsilon N(\varepsilon)\tau(\varepsilon)$. In taking the derivative of $\sigma(\epsilon)$ with respect to ϵ, only the delta function inside the integral is actually differentiated. After an integration by parts we get

$$\frac{\partial\sigma(\varepsilon)}{\partial\varepsilon}=\frac{2e^2}{3m}\frac{\partial h(\varepsilon)}{\partial\varepsilon}\ . \tag{C3}$$

Furthermore, in an isotropic scattering model, the scattering rate is given by

$$\frac{1}{\tau(\varepsilon_\mathbf{k})}=\sum_{\mathbf{k}'}W_{\mathbf{k}\mathbf{k}'}\frac{k_z-k_z'}{k_z}\ , \tag{C4}$$

where the transition probability is

$$W_{\mathbf{k}\mathbf{k}'}=\frac{2\pi}{\hbar}N_{\rm imp}P(\,|\,\mathbf{k}-\mathbf{k}'\,|\,;\varepsilon_k,\varepsilon_k')\delta(\varepsilon_\mathbf{k}-\varepsilon_\mathbf{k}')\ . \tag{C5}$$

The function P is basically proportional to the square of the pseudopotential times a structure function. As seen explicitly in (C5), the transition probability depends only on the angle between $\mathbf{k}$ and $\mathbf{k}'$. Once the angular integrals are completed, the scattering rate simplifies to

$$\frac{1}{\tau(\varepsilon_\mathbf{k})}=\Omega\frac{2\pi}{\hbar}N_{\rm imp}\tfrac{1}{4}\int d\epsilon_{\mathbf{k}'}N(\varepsilon_{\mathbf{k}'})\delta(\varepsilon_\mathbf{k}-\varepsilon_{\mathbf{k}'})F(\varepsilon_\mathbf{k},\varepsilon_{\mathbf{k}'})\ , \tag{C6}$$

where

$$F(\varepsilon_\mathbf{k},\varepsilon_\mathbf{k}')=\int_{-1}^{1}dx(1-x)P(z;\varepsilon_\mathbf{k},\varepsilon_\mathbf{k}')\ , \tag{C7}$$

and $z=(2m/\hbar^2)[\varepsilon_\mathbf{k}+\varepsilon_\mathbf{k}'-2(\varepsilon_\mathbf{k}\varepsilon_\mathbf{k}')^{1/2}x]$. The variation of (C6) with respect to $\varepsilon_\mathbf{k}$ can be obtained easily and equals

$$\frac{\partial}{\partial\varepsilon_\mathbf{k}}\frac{1}{\tau(\varepsilon_\mathbf{k})}=\Omega\frac{2\pi}{\hbar}N_{\rm imp}\frac{1}{4}\frac{\partial}{\partial\varepsilon_\mathbf{k}}[N(\varepsilon_\mathbf{k})G(\varepsilon_\mathbf{k})]\ , \tag{C8}$$

where $G(\varepsilon_\mathbf{k})$ is the equal energy component of (C7) defined as

$$G(\varepsilon)=F(\varepsilon,\varepsilon)=8\int_0^1 dy\,y^3P(2ky;\varepsilon,\varepsilon)\ . \tag{C9}$$

On substituting (C8) in (C3) to obtain the derivative of the conductivity with respect to $\varepsilon_\mathbf{k}$, the dimensionless thermopower ξ defined in (2.10) then becomes

$$\xi=1-\left[\varepsilon\frac{G'(\varepsilon)}{G(\varepsilon)}\right]_{\varepsilon=\varepsilon_F}\ . \tag{C10}$$

Equation (C10) can be further simplified and reduces to

$$\xi=3-\frac{4P(2k;\varepsilon,\varepsilon)}{G(\varepsilon)}-\frac{8\varepsilon\int_0^1 dy\,y^3(\partial P/\partial\varepsilon)}{G(\varepsilon)}\ . \tag{C11}$$

If, as is the case in this paper, the pseudopotential is not energy dependent, only the first two terms are present in (C11).

[1] L. J. Brillson, Surf. Sci. Rep. **2**, 123 (1982).

[2] *Synthetic Modulated Structures,* edited by L. L Chang and B. C. Giessen (Academic, New York, 1985).

[3] I. K. Schuller, Phys. Rev. Lett. **44**, 1597 (1980).

[4] W. P. Lowe, T. W. Barbee, T. H. Geballe, and D. B. McWhan, Phys. Rev. B **24**, 6193 (1981).

[5] S. M. Durbin, J. E. Cunningham, and C. P. Flynn, J. Phys. F **12**, L75 (1982).

[6] P. F. Carcia and A. Suna, J. Appl. Phys. **54**, 2000 (1983).

[7] K. Ploog and G. H. Dohler, Adv. Phys. **32**, 285 (1983); A. C. Gossard, IEEE J. Quantum Electron **QE-22**, 1649 (1986).

[8] For the case of Al-Si see, for example, R. Rosenberg, M. J. Sullivan, and J. K. Howard, in *Thin Films— Interdiffusion and Reactions,* edited by J. M. Poate, K. N. Tu, and J. W. Mayer (Wiley-Interscience, New York, 1978), p. 13.

[9] T. R. Werner, I. Banerjee, Q. S. Yang, C. M. Falco, and I. K. Schuller, Phys. Rev. B **26**, 2224 (1982).

[10] J. Q. Zheng, J. B. Ketterson, C. M. Falco, and I. K. Schuller, Physica B&C **108**, 945 (1981).

[11] K. Fuchs, Proc. Cambridge Phil. Soc. **34**, 100 (1938).

[12] E. H. Sondheimer, Adv. Phys. **1**, 1 (1952).

[13] P. A. Lee and T. V. Ramakrishnan, Rev. Mod. Phys. **57**, 287 (1985).

[14] S. Doniach and E. H. Sondheimer, *Green's Functions for Solid State Physicists* (Benjamin, Massachusetss, 1974).

[15] J. P. Hansen and I. R. McDonald, *Theory of Simple Liquids* (Academic, New York, 1976).

[16] N. W. Ashcroft and N. D. Mermin, *Solid State Physics* (Holt, Rinehart and Winston, New York, 1976), p. 322.

[17] D. Pines and P. Nozières, *The Theory of Quantum Liquids* (Benjamin, New York, 1966).

[18] See N. W. Ashcroft and N. D. Mermin, *Solid State Physics,* Ref. 16, p. 326.

[19] W. E. Lawrence and L. A. Cole, J. Phys. F **15**, 883 (1985).

[20] P. T. Coleridge, J. Phys. F **2**, 1016 (1972).

[21] J. W. Blaker and R. Harris, J. Phys. C **4**, 569 (1971).

[22] R. S. Sorbello, J. Phys. F **4**, 1665 (1974).

[23] E. H. Sondheimer, Proc. R. Soc. London, Ser. A **268**, 100 (1962).

[24] J. M. Ziman, *Electrons and Phonons* (Oxford University Press, London, 1960), article (7.7).

[25] J. M. Ziman, *Principles of the Theory of Solids,* 2nd ed. (Cambridge University Press, Cambridge, England 1972), article (7.5).

[26]See J. M. Ziman, *Electrons and Phonons,* Ref. 24, article (9.12).

[27]G. V. Chester and A. Thellung, Proc. Phys. Soc., London, **77**, 1005 (1961).

[28]J. M. Ziman, Adv. Phys. **16**, 551 (1967).

[29]The assumption of a weak pseudopotential is not directly applicable to transition metals. For an extension of the pseudopotential concept to include these metals see J. A. Moriarty, Phys. Rev. B **6**, 1239 (1972).

[30]The additional effect of the average superlattice potential on the dispersion relation is to produce gaps which are diminished over those of the original metal. If we assume typical values for $\varepsilon_F \sim 5$ eV and for the lattice constant in the host metal $a \sim 5$ Å, then $\varepsilon_{\text{gap}}^{\text{SL}}/\varepsilon_F = (\varepsilon_{\text{gap}}^{\text{metal}}/\varepsilon_F)(a/d) \sim 0.2a/d$, where the gap in the host metal is taken to be of the order of 1 eV. Since d is typically 20—100 Å, the above ratio is ~ 0.001—0.05. Hence the effect of the superlattice potential can be neglected.

[31]Strictly speaking, the scattering centers, though quenched, are nonetheless dynamic objects. Thus the scattering cross section is properly given by $S(q,\omega)$, the dynamic structure factor. However, we shall assume that if we are at sufficiently high temperatures, the sum over all final states leads to the usual static limit, i.e., $S(q)$.

[32]N. W. Ashcroft and J. Lekner, Phys. Rev. **145**, 83 (1966).

[33]J. K. Percus and G. J. Yevick, Phys. Rev. **110**, 1 (1958).

[34]F. Lado, J. Chem. Phys. **49**, 3092 (1968).

[35]M. L. Cohen and V. Heine, Solid State Phys. **24**, 37 (1970).

[36]D. G. Pettifor and M. A. Ward, Solid State Commun. **49**, 291 (1984).

[37]J. D. Bernal, Proc. R. Soc. London, Ser. A **280**, 299 (1964).

[38]G. J. Galvin, M. O. Thompson, J. W. Mayer, R. B. Hammond, N. Paulter, and P. S. Peercy, Phys. Rev. Lett. **48**, 33 (1982).

[39]A. F. Mayadas and M. Shatzkes, Phys. Rev. B **1**, 1382 (1970).

[40]A. F. Ioffe and A. R. Regel, Prog. Semicond. **4**, 237 (1960).

[41]I. Nakamichi and T. Kino, Trans. Jpn. Inst. Met. **27**, Suppl. 1013 (1986).